

On the inverse energy transfer in rotating turbulence

Michele Buzdicotti¹, Patricio Clark Di Leoni¹ and Luca Biferale¹

Department of Physics & INFN, University of Rome ‘Tor Vergata’, Via della Ricerca Scientifica 1, 00133 Rome, Italy

Received: date / Revised version: date

Abstract. Rotating turbulence is an example of a three-dimensional system in which an inverse cascade of energy, from the small to the large scales, can be formed. While usually understood as a byproduct of the typical bidimensionalization of rotating flows, the role of the three-dimensional modes is not completely comprehended yet. In order to shed light on this issue, we performed direct numerical simulations of rotating turbulence where the 2D modes falling in the plane perpendicular to rotation are removed from the dynamical evolution. Our results show that while the two-dimensional modes are key to the formation of a stationary inverse cascade, the three-dimensional degrees of freedom play a non-trivial role in bringing energy to the larger scales also. Furthermore, we show that this backwards transfer of energy is carried out by the homochiral channels of the three-dimensional modes.

PACS-keydescribing text of that key – PACS-key describing text of that key

1 Introduction

In the classical picture of three dimensional turbulence, energy is injected in the larger scales of the problem and then transferred to the smaller ones in a process known as a direct energy cascade [1,2,3]. Since Richardson’s observations and Kolmogorov’s prediction turbulent cascades have been studied in many systems, e.g. in rotating flows, stratified flows, and magnetohydrodynamics flows [4]. One of the most important results so far has been Kraichnan’s prediction [5] of the presence of an *inverse* cascade of energy in two dimensional turbulence. Under this regime, energy flows from small to large scales. Later, inverse cascades have also been studied in three dimensional systems such as rotating flows [6,7,8], shallow fluid layers [9,10], oceanic flows [11], magnetohydrodynamics [12,13], and helically decimated flows [14,15,16]. While in two dimensional turbulence the inverse energy transfer can be predicted and understood by the presence of two positive definite quadratic inviscid invariants, namely energy and enstrophy, the same argument cannot be extended to the three dimensional systems, where the second quadratic inviscid invariant, helicity, is not sign definite. Understanding how inverse cascades are formed in three dimensional problems is the subject of ongoing research.

In this work we focus on the case of rotating turbulence. Flows under rotation present a rich phenomenology with plenty of physical interest, moreover they are common in nature, e.g. in the atmosphere and in the oceans [17], in planetary cores [18], as well as in several engineering problems [19]. The presence of the Coriolis force in

these flows breaks isotropy [20], generates inertial waves and gives rise to the formation of large scales columnar vortices [4,21]. The resulting flows look almost bidimensional, with most of the energy accumulated in the modes perpendicular to the rotation axis, as seen in simulations [6,22] and experiments [23]. These effects happen because the nature of the nonlinear interactions is changed [24,25] with the appearance of resonant interactions due to the action of the inertial waves in the turbulent flow [26]. Resonant interactions are known to play an important role in turbulent dynamics [27,28,29], and their action has been studied directly in experiments [30,31] and simulations [32,33,34]. While it can be shown that the effect of resonant interactions can make the energy transfer anisotropic, with energy being preferentially transferred to modes closer and closer to the plane perpendicular to the rotation axis, it can also be shown that they cannot transfer energy directly into the perpendicular plane [35]. Furthermore, the modes perpendicular to the rotation axis (the 2D modes, because of their two-dimensional nature) and the resonant triads are decoupled under strong rotation [35]. So the question of how the transfer of energy between the 2D and the rest of the modes (the 3D modes, as they encompass all three-dimensional modes in the flow) takes place remains open [21,36], with eddies [37,23] and quasi-resonant interactions [38,39] appearing to have an important role in the rotating turbulence dynamics. Of particular interest to the present work are the simulations done by [18], where they showed that if the 2D modes are damped, the system then enhances the creation of waves and small scale structures, suggesting that the balance between 2D and 3D modes is indeed delicate and dynamic. A similar experiment was also performed in convective flows [40]. It is important to stress that in nu-

merical simulations on a finite-box domain exact resonant interactions may be “lost” due to discretization effects at small wavenumbers [41], thus making quasi-resonant interactions even more important at the large scales [42, 43].

The phenomenon of bidimensionalization is an important one because the inverse cascade in rotating flows is often seen as a byproduct of the emerging 2D dynamics [6,7,8]. In this picture, the decoupled modes behave as purely 2D and Kraichnan’s result is recovered [5]. As can be expected, wave turbulence theories prohibit the formation of 2D solutions [41]. In these theories, the transfer of energy towards the 2D manifold becomes too weak to trigger an inverse cascade. It should be noted, nonetheless, that it can be shown that bidimensionalization can be achieved in periodic domains in the low Rossby limit [39]. All things considered, this scenario begs many questions: if there is some coupling between the 2D and the 3D modes that is able to put energy from the former to the latter, then wouldn’t this coupling also work the other way? If resonant interactions can make the energy transfer anisotropic, aren’t they also contributing to the inverse transfer of energy? Moreover, it has been shown that even in fully homogeneous and isotropic three dimensional turbulence, there are channels that take energy backwards [14,15], that the action of these channels can be enhanced in different geometries [44], and that these channels can couple the 2D and 3D modes in rotating turbulence [36]. This adds a further avenue to explore.

In order to better understand the mechanisms behind the inverse cascade in rotating turbulence we perform simulations where the two dimensional modes are conservatively removed and compare them to a simulation of the full Navier-Stokes equations. In this way the flow can never, by construction, become two dimensional, therefore all the purely three-dimensional effects involved in the inverse energy transfer come into light. The results show that although a stationary inverse cascade is not formed, energy is nonetheless transferred and accumulated in modes larger than the ones where it is injected. A pseudo-bidimensionalization takes place where energy is condensated in the lowest wavenumbers close to the perpendicular plane, forming a quasi 2D flow. In these states, the homochiral channels of the energy flux bring the energy to the large scales while the heterochiral ones bring it to the small scales, with the two of them balancing out. In summary, our results show that while the 2D modes are key to the formation of an inverse cascade in rotating flows, the 3D modes play a non-negligible role in the distribution of energy, making the overall dynamics very rich.

The paper is organized as follows, in Sec. 2 we introduce the equations of rotating turbulence and several of its core concepts, explain the process used to keep only the three-dimensional modes, and give details on the simulations we perform and the different quantities we analyze, in Sec. 3 we present the results coming from our numerical simulations, and in Sec. 4 we give concluding remarks.

2 Rotating turbulence equations

The governing equations for an incompressible fluid in a rotating frame can be written as

$$\begin{cases} \partial_t \mathbf{u} + \boldsymbol{\omega} \times \mathbf{u} + 2\boldsymbol{\Omega} \times \mathbf{u} = -\nabla p + \nu \Delta \mathbf{u} + \mathbf{f} \\ \nabla \cdot \mathbf{u} = 0, \end{cases} \quad (1)$$

where ν is the kinematic viscosity, \mathbf{f} is an external forcing, the term $2\boldsymbol{\Omega} \times \mathbf{u}$ is the Coriolis force produced by rotation, and $\boldsymbol{\Omega} = \Omega \hat{z}$ is the angular velocity with frequency Ω around the rotation axis \hat{z} . The fluid density is constant and absorbed into the definition of pressure p .

Taking the curl of the linearized form of Eq. (1) in the dissipation- and force-less regime (i.e., $\nu = 0$ and $\mathbf{f} = 0$) yields

$$\partial_t (\nabla \times \mathbf{u}) = 2 (\boldsymbol{\Omega} \cdot \nabla) \mathbf{u}. \quad (2)$$

The general solution of this equation is given by a superposition of waves of the form

$$\mathbf{u}(\mathbf{x}, t) = \sum_{\mathbf{k}, s_k} \mathbf{h}_{s_k}(\mathbf{k}) e^{i[\mathbf{k} \cdot \mathbf{x} - \omega_{s_k}(\mathbf{k})t]} \quad (3)$$

where $s_k = \pm$, $\mathbf{h}_{s_k}(\mathbf{k})$ are the orthogonal eigenmodes of the curl operator, $i\mathbf{k} \times \mathbf{h}_{s_k} = s_k k \mathbf{h}_{s_k}$ [45], and the wave frequencies, ω_{s_k} , are given by the dispersion relation,

$$\omega_{s_k}(\mathbf{k}) = s_k 2\Omega \frac{k_z}{|\mathbf{k}|}, \quad (4)$$

where k_z is the direction of the rotation axis. These are the aforementioned inertial waves. It follows that, for each wavevector there are two waves with opposite sign of helicity. The right-handed wave propagating in the direction of \mathbf{k} and the left-handed wave propagating in the $-\mathbf{k}$ direction. Inertial waves also bring resonant triads into play. It is well known that in Eq. (1), Fourier modes interact in triads satisfying $\mathbf{k} + \mathbf{p} + \mathbf{q} = 0$, where \mathbf{k} , \mathbf{p} , and \mathbf{q} are the three wavevectors involved in the triad. The presence of inertial waves adds a second condition

$$\omega_{s_k}(\mathbf{k}) + \omega_{s_p}(\mathbf{p}) + \omega_{s_q}(\mathbf{q}) = 0, \quad (5)$$

known as the resonance condition. Resonant interactions are very important to the evolution of a rotating turbulent flow, but they do not encompass all of the interactions that happen in it [32,34].

The Reynolds and the Rossby numbers are the two non-dimensional parameters which control the dynamic evolution of the flow. They can be written, respectively, as

$$Re = \frac{UL_f}{\nu}, \quad Ro = \frac{U}{2\Omega L_f}, \quad (6)$$

where $L_f \sim 1/k_f$ is the forcing scale, and U is the rms velocity at the forcing scale. The Rossby number represents the ratio between the Coriolis force and inertial forces in the flow. In the limit of large Rossby numbers, $Ro \gg 1$,

the flow can evolve freely under its own internal dynamics without being influenced by rotation. In the $Ro \lesssim 1$ regime, we can expect to observe effects of rotation on the flow.

2.1 Rotating turbulence on a reduced Fourier set

From the dispersion relation in Eq. (4) it is clear that all wavenumbers lying in the Fourier space plane, $(k_x, k_y, k_z = 0)$, perpendicular to the rotation axis, do not give rise to inertial waves, as $\omega_{s_k}(\mathbf{k}_\perp) = 0$. These are the aforementioned 2D modes, with all the rest of the modes in the system being the 3D modes. The two sets can be written explicitly in the following way

$$\mathbf{k}_{2D} = \{\forall \mathbf{k} \mid k_z = 0\}, \quad (7)$$

$$\mathbf{k}_{3D} = \{\forall \mathbf{k} \mid k_z \neq 0\}, \quad (8)$$

with \mathbf{k}_{2D} being the set of the 2D modes, and \mathbf{k}_{3D} the one of the 3D modes. The 2D and 3D modes sets are sometimes referred to as the “slow” and “fast” manifolds, respectively [46, 47, 48].

As mentioned above, in turbulence under rotation energy tends to accumulate in the 2D modes [8]. But it is not clear whether the inverse cascade is produced only due to the action of these modes, or if the 3D modes also play a role. In this work, we directly investigate the role of the 3D modes in the energy transfer. To do this, we reduce the set of possible interactions described in the system of Eqs. (1) to only the interactions which couple modes inside the 3D set. Restricting the dynamics of Eq. (1) to only the 3D modes can be accomplished by using a generalized Galerkin projector, \mathcal{P} , which acts on the velocity field as follows:

$$\mathbf{v}(\mathbf{x}, t) = \mathcal{P} \mathbf{u}(\mathbf{x}, t) = \sum_{\mathbf{k}} e^{i\mathbf{k} \cdot \mathbf{x}} \gamma_{\mathbf{k}} \hat{\mathbf{u}}(\mathbf{k}, t), \quad (9)$$

where $\mathbf{v}(\mathbf{x}, t)$ is the representation of the decimated velocity field in the real space. The factors $\gamma_{\mathbf{k}}$ are chosen to be either 1 or 0 with the following rule:

$$\gamma_{\mathbf{k}} = \begin{cases} 1, & \text{if } \mathbf{k} \in \mathbf{k}_{3D} \\ 0, & \text{if } \mathbf{k} \in \mathbf{k}_{2D}. \end{cases} \quad (10)$$

In this way the only active modes are the one inside the 3D set. Moreover, the factors $\gamma_{\mathbf{k}}$ preserve Hermitian symmetry $\gamma_{\mathbf{k}} = \gamma_{-\mathbf{k}}$ so that \mathcal{P} is a self-adjoint operator. The resulting equations for the Fourier decimated velocity field are then,

$$\begin{cases} \partial_t \mathbf{v} = \mathcal{P}[-\nabla p - (\mathbf{v} \cdot \nabla \mathbf{v})] - 2\boldsymbol{\Omega} \times \mathbf{v} + \nu \Delta \mathbf{v} + \mathcal{P} \mathbf{f} \\ \nabla \cdot \mathbf{v} = 0. \end{cases} \quad (11)$$

In the above definition of the decimated equations, the nonlinear term must be projected on the quenched decimated set, to constrain the dynamical evolution to evolve

on the same set of Fourier modes at all times. Moreover it is important to see that the resulting dynamics still conserves total energy and helicity. Similarly, any initial condition and the external forcing used must have a support on the same decimated set of Fourier modes only.

2.2 Energy spectra and fluxes

We now define the different energy spectra and fluxes we use in this study. The isotropic energy spectrum of the 3D modes can be written as

$$E(k) = \frac{1}{2} \sum_{k \leq |\mathbf{k}| < k+1} |\hat{\mathbf{v}}(\mathbf{k})|^2. \quad (12)$$

We can further decompose the spectrum into two components, one parallel and one perpendicular

$$e(k_\perp, k_\parallel) = \frac{1}{2} \sum_{\substack{k_\perp \leq |\mathbf{k} \times \hat{z}| < k_\perp + 1 \\ k_\parallel \leq k_z < k_\parallel + 1}} |\hat{\mathbf{v}}(\mathbf{k})|^2, \quad (13)$$

with $k_\perp = \sqrt{k_x^2 + k_y^2}$ and $k_\parallel = k_z$. This spectrum takes into account the anisotropic nature of the flow. When plotting $e(k_\perp, k_\parallel)$, a trigonometric factor of $1/\sin \theta$, with $\theta = \arctan k_\parallel/k_\perp$, will always be included. Otherwise, even in the isotropic case (i.e., $\Omega = 0$) the spectrum (13) would not look isotropic, as there are many more modes with low θ entering in the summation.

The total energy flux has the form

$$\Pi(k) = - \sum_{|\mathbf{k}| \leq k} ik_j \hat{v}_i(-\mathbf{k}) \sum_{\mathbf{p}, \mathbf{q}} \hat{v}_i(\mathbf{p}) \hat{v}_j(\mathbf{q}) \delta(\mathbf{p} + \mathbf{q} - \mathbf{k}). \quad (14)$$

Notice that the decimated velocity $\hat{\mathbf{v}}(\mathbf{k})$ is non-zero only when $\mathbf{k} \in \mathbf{k}_{3D}$, so the flux only takes into account the interactions of the 3D modes.

The energy flux can be further analyzed in terms of its homochiral and heterochiral components. Doing this is important because it is known that homochiral triads are responsible of opening a channel that takes energy from the small to the large scales, even in 3D homogeneous and isotropic turbulence [16, 49]. So in the context of rotating turbulence it is interesting to see if rotation is only producing a decoupling between 2D and 3D modes (whereby the inverse cascade is then a product of the 2D dynamics), or if it also enhances the backward flux produced by the homochiral interactions inside the 3D manifold. To calculate the homo and heterochiral energy fluxes, we first decompose the velocity field into the helical modes, \mathbf{h}_+ and \mathbf{h}_- , defined above, as proposed by [50, 51], in order to obtain

$$\begin{aligned} \hat{\mathbf{v}}(\mathbf{k}, t) &= \hat{\mathbf{v}}^+(\mathbf{k}, t) + \hat{\mathbf{v}}^-(\mathbf{k}, t) \\ &= \hat{\mathbf{v}}^+(\mathbf{k}, t) \mathbf{h}_+(\mathbf{k}) + \hat{\mathbf{v}}^-(\mathbf{k}, t) \mathbf{h}_-(\mathbf{k}). \end{aligned} \quad (15)$$

It is important to note that this decomposition can be performed for any three dimensional incompressible field,

not just for the case of rotating flows. Under this change of basis, we can write the energy flux corresponding to triads in which all modes have the same sign of the helicity, the homochiral, and those in which one mode has a different sign, the heterochiral. The corresponding homochiral ($\Pi^{\text{HO}}(k)$) and heterochiral ($\Pi^{\text{HE}}(k)$) energy fluxes can then be defined as:

$$\Pi^{\text{HO}}(k) = - \sum_{\substack{|\mathbf{k}| \leq k, \\ \mathbf{q} = \mathbf{k} - \mathbf{p}}} [\hat{\mathbf{v}}^+(-\mathbf{k}) \cdot (i\mathbf{k} \cdot \hat{\mathbf{v}}^+(\mathbf{p}))\hat{\mathbf{v}}^+(\mathbf{q}) + \hat{\mathbf{v}}^-(-\mathbf{k}) \cdot (i\mathbf{k} \cdot \hat{\mathbf{v}}^-(\mathbf{p}))\hat{\mathbf{v}}^-(\mathbf{q})], \quad (16)$$

$$\Pi^{\text{HE}}(k) = \Pi(k) - \Pi^{\text{HO}}(k), \quad (17)$$

where $\Pi(k)$ is the total energy flux defined in Eq. (14).

2.3 Numerical simulations

As we are interested in the physics of the inverse cascade, we study the flows defined above using hyperviscous dissipation, so as to reduce the range of scales affected by viscosity. In this way, Eqs. (1) become

$$\begin{cases} \partial_t \mathbf{u} = -\nabla p - \boldsymbol{\omega} \times \mathbf{u} - 2\boldsymbol{\Omega} \times \mathbf{u} + \nu(-1)^{\alpha+1} \Delta^\alpha \mathbf{u} + \mathbf{f} \\ \nabla \cdot \mathbf{u} = 0, \end{cases} \quad (18)$$

and Eqs. (11)

$$\begin{cases} \partial_t \mathbf{v} = \mathcal{P}[-\nabla p - (\mathbf{v} \cdot \nabla \mathbf{v})] - 2\boldsymbol{\Omega} \times \mathbf{v} + \nu(-1)^{\alpha+1} \Delta^\alpha \mathbf{v} + \mathcal{P} \mathbf{f} \\ \nabla \cdot \mathbf{v} = 0. \end{cases} \quad (19)$$

We perform direct numerical simulations of Eqs. (19) in a triple periodic domain with a fully dealiased parallel 3D pseudospectral code using grids of up to $N^3 = 512^3$ collocation points. The time integration has been performed with the second-order Adams-Bashforth scheme with the viscous term integrated implicitly. The external forcing, \mathbf{f} , is a delta correlated random process in Fourier space

$$\langle \hat{\mathbf{f}}(\mathbf{k}) \hat{\mathbf{f}}^*(\mathbf{q}) \rangle = F(\mathbf{k}) \delta_{\mathbf{k}, \mathbf{q}} \hat{\mathbf{Q}}(\mathbf{k}), \quad (20)$$

where $F(\mathbf{k})$ is an amplitude term that only has support around k_f and $\hat{\mathbf{Q}}(\mathbf{k})$ is a projector applied to guarantee incompressibility. The values of the different parameters used are presented in Table 1. It is known that hyperviscosity introduces a bottleneck in the energy spectrum close to the dissipative scales, however, for the interests of this work, namely the properties of the backward energy transfer from the forcing to the large scales, we can safely assume that the spurious effects of hyper-viscous dissipation are negligible.

The simulations can be distinguished in two different sets. In the first, PRJ-A, we fix the forcing properties and

Simulation	Projected	N	Ω	k_f	ε	Ro
FULL	No	256	80	30	0.045	0.008
PRJ-A1	Yes	256	0	30	0.06	∞
PRJ-A2	Yes	256	5	30	0.06	0.1
PRJ-A3	Yes	256	15	30	0.06	0.04
PRJ-A4	Yes	256	40	30	0.06	0.025
PRJ-A5	Yes	256	80	30	0.06	0.015
PRJ-A6	Yes	256	160	30	0.06	0.009
PRJ-B1	Yes	256	80	4	0.4	0.007
PRJ-B2	Yes	256	80	15	0.1	0.011
PRJ-B3	Yes	256	80	30	0.06	0.015
PRJ-B4	Yes	512	80	50	1.2	0.03

Table 1. Parameters used in the different simulations. ‘‘Projected’’ indicates if the full equations (Eqs. (18)) or the projected ones (Eqs. (19)) are used; N : number of collocation points in each spatial direction; Ω : rotation rate; k_f : forced wavenumbers; ε : viscous energy dissipation; $Ro = (\varepsilon_f k_f^2)^{1/3} / \Omega$: Rossby number defined in terms of the energy injection properties. In all simulations the order of the Laplacian $(-1)^{\alpha+1} \nu \Delta^\alpha \mathbf{v}$ is set to $\alpha = 4$, and the kinematic viscosity to $\nu = 1.8 \times 10^{-13}$, except for the simulation with resolution $N = 512$, where the viscosity is set equal to $\nu = 7.1 \times 10^{-14}$.

we study the system at changing the rotation rate Ω . In the second set, PRJ-B, we study the effects of changing the forcing scale, keeping the same rotation rate. In particular, in set PRJ-A, we keep the energy input fixed at $k_f = 30$, which guarantees a large enough inverse inertial range, and vary Ω between 0 and 160. In set PRJ-B, instead, we fix $\Omega = 80$, which ensures a rotation rate strong enough to produce backward cascade, and we change the input scales from $k_f = 4$ up to $k_f = 50$. For this last simulation, we increase the resolution up to $N^3 = 512^3$, in order to be able to force at $k_f = 50$. As a control and benchmark, we also perform a simulation of the original non-decimated system (Eqs. (18)), which we refer to as FULL. In order to make a fair comparison with the other simulations, we only force the 3D modes so as to not inject energy directly into the 2D ones. More details about all the simulations are reported in Table 1.

3 Results

In Fig. 1 we show visualizations of the absolute value of the velocity for three simulations: PRJ-A1, PRJ-A5, and FULL (which have $\Omega = 0$, $\Omega = 80$ and $\Omega = 80$, and are shown in panels A, B and C, respectively). As expected, simulation PRJ-A1 shows the typical disordered structures found in homogeneous isotropic turbulence and simulation FULL shows the characteristic columnar vortices with vertical symmetry of rotating flows. On the other hand, PRJ-A5 shows vertical structures that resemble the columnar vortices, but with no vertical symmetry and with a stronger presence of disordered three-dimensional structures. In a way, it is as if the system is trying to build the columnar vortices but it is not able to successfully do it.

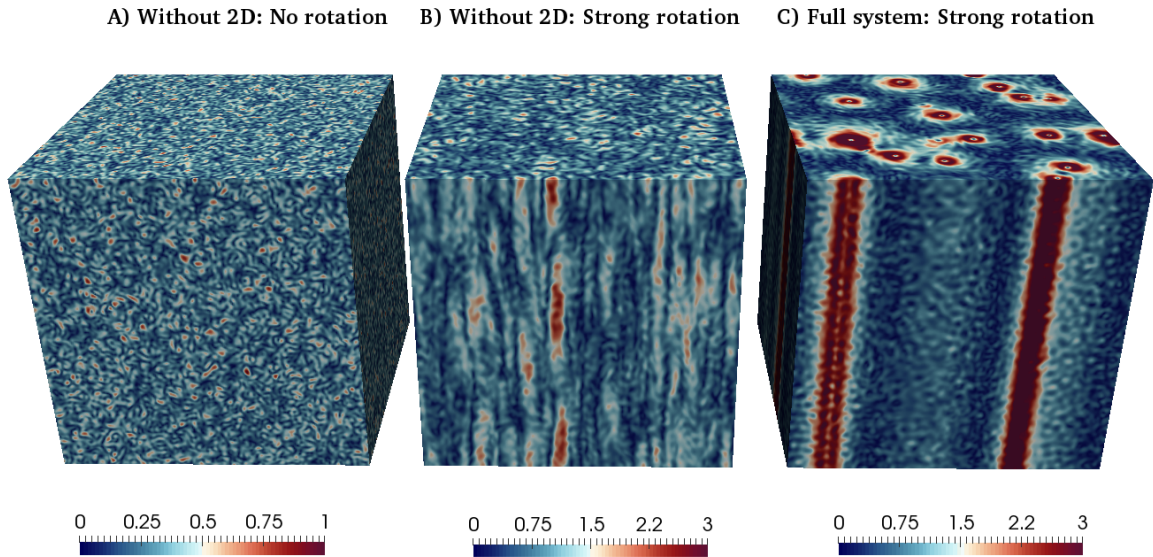


Fig. 1. Visualizations of the absolute value of the velocity field for three simulations: A) projected system without the 2D manifold with no rotation (simulation PRJ-A1), B) projected system without the 2D manifold with strong rotation (simulation PRJ-A5), and C) the full system with strong rotation (simulation FULL).

Moving on to a more quantitative analysis, in Fig. 2 we present the total energy evolution for the set of decimated simulations PRJ-A and for the simulation FULL, where we retain the 2D modes. It is evident that only keeping the 3D modes strongly affects the dynamical evolution of the resulting systems. In particular, comparing the evolution of FULL with that of PRJ-A5, we can see that in the case of full Navier-Stokes equations the total energy increases with a constant speed as a function of time, while in the decimated system the total energy grows linearly only in a first transient of time, then it saturates to a stationary state. This result suggests that without the 2D modes the system is not able to establish a backward energy transfer stationary in time. From the same Fig. 2 we can also assess the effect of changing the Rossby number on the evolution of the decimated systems. In particular we can see that if Rossby is large enough, namely when $\Omega \leq 5$, the system does not seem to show a transient period with constant energy increase, while this does happen when $\Omega > 5$.

In order to have a better understanding of how energy is distributed in the system with 3D modes only, we show in Fig. 3 the energy spectra for the simulations in PRJ-A and for the simulation FULL. The spectra of the decimated simulations is averaged on time once they reach their stationary regime, while the spectra from simulation FULL is not averaged in time, as it never reaches a stationary state. If rotation is not strong enough, energy is not transferred to the smaller wavenumbers, as suggested in Fig. 2. But if rotation is strong, energy is indeed transferred to modes with $k < k_f$ even though there are no 2D

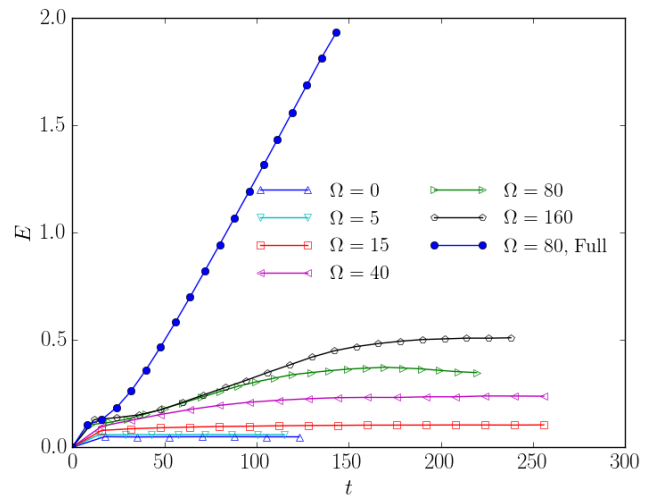


Fig. 2. Evolution of total energy as a function of time for the set of simulations without the 2D manifold, PRJ-A, for different values of Ω . For comparison the total energy evolution for the non-decimated (simulation FULL) system is also present (circular full markers).

modes in the system. Interestingly, two distinct peaks are formed around $10 \leq |\mathbf{k}| \leq 12$ and around $5 \leq |\mathbf{k}| \leq 7$. While the position of these peaks does not seem to be greatly affected by the rotation rate, their amplitude is, with larger values of Ω generating bigger peaks. These peaked spectra differ greatly from the equipartition spec-

trum k^2 . It is important to note that there is no kind of large scale friction being used in these simulations, so, as we will see below, the total energy flux of the decimated cases in the region $k < k_f$ must be zero.

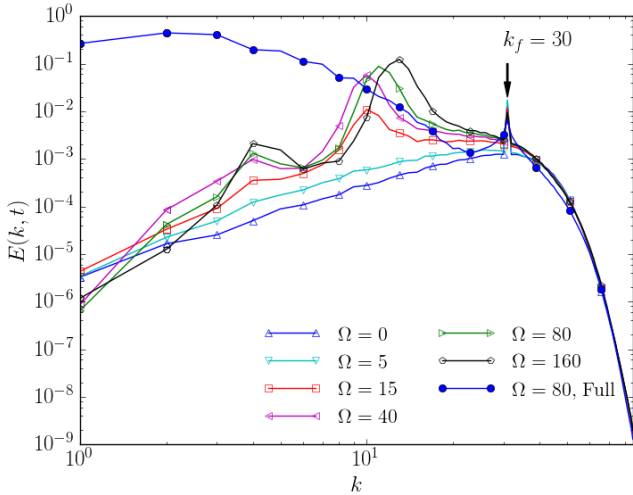


Fig. 3. Energy spectra for the simulations without the 2D manifold, PRJ-A, at changing Ω . For comparison the energy spectrum for the non-decimated (simulation FULL) system is also present (circular full markers).

Figure 4 shows the energy spectra of the simulations in set PRJ-B, where we keep the rotation rate fixed at $\Omega = 80$ and vary the forcing scale k_f . In all cases, energy is accumulated around the same peaks seen in Fig. 3, even for the case of PRJ-B1, where the forcing is acting on wavenumbers smaller than those where the peak is formed.

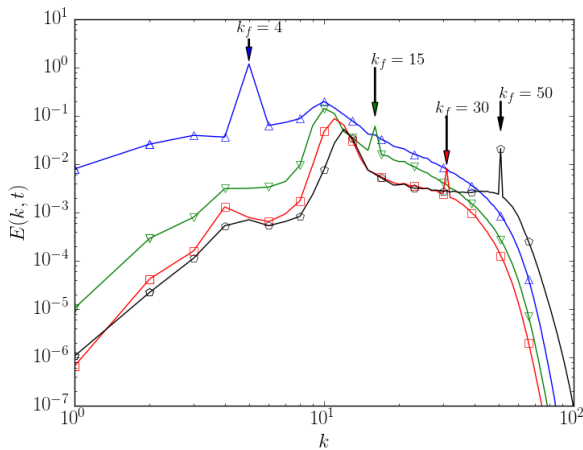


Fig. 4. Energy spectra $E(k)$ of the simulations in set PRJ-B.

So as to understand how the energy is distributed among modes parallel and perpendicular to the rotation axis, in Fig. 5, we analyze the decomposed energy spectra $e(k_\perp, k_\parallel)$ of the simulations PRJ-A1, PRJ-A5, and

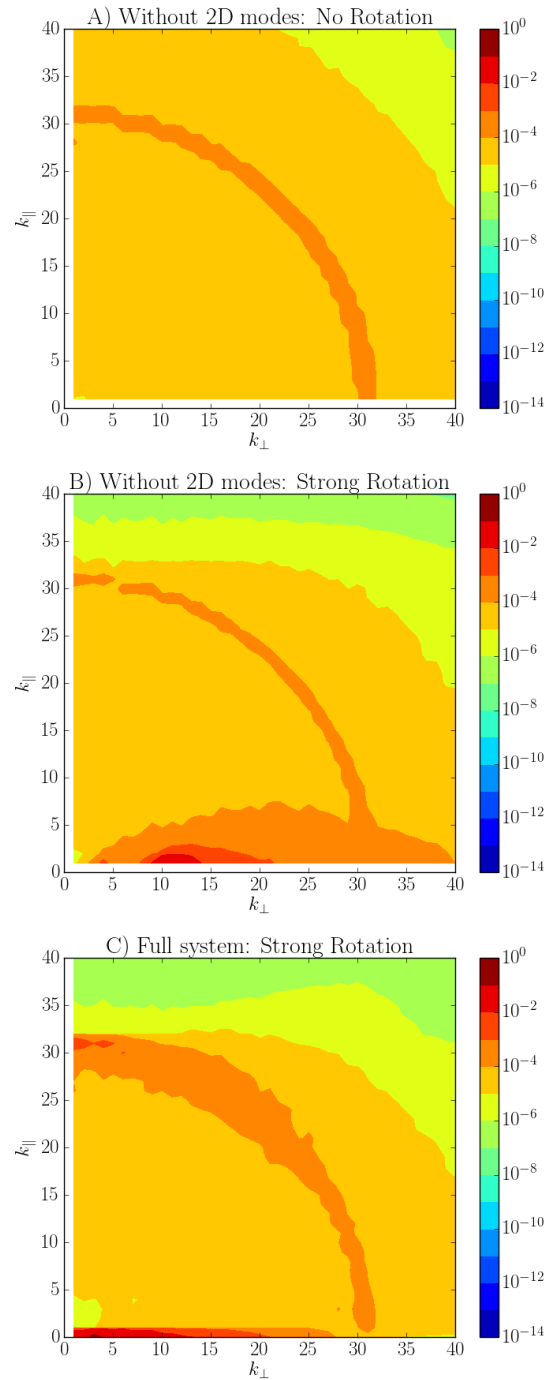


Fig. 5. Decomposed energy spectra $e(k_\perp, k_\parallel)$ of simulations: A) PRJ-A1, B) PRJ-A5 and C) FULL.

FULL. In the non-rotating case, PRJ-A1 shown in panel A, the spectral energy density forms concentric circles centered around $k = 0$ in an isotropic fashion. On the other hand, when rotation is active this distribution becomes anisotropic, with a stronger accumulation of energy in modes with low k_\parallel , as expected from [35]. While in simulation FULL (shown in panel C) energy is indeed located in the 2D modes as commonly happens in rotating turbulence, in simulation PRJ-A5 (shown in panel B) energy

goes towards modes with low k_{\parallel} but is then squashed between $k = 1$ and $k = 5$, as it cannot go to the 2D modes. So, the action of the 3D modes does take energy to the larger scales and with a preference towards modes close to the 2D modes. It is important to note that in simulation FULL, no energy is being injected directly into the 2D modes. So while resonant interactions make the spectra evolution anisotropic, quasi-resonant interactions must be coming into play in order to couple the 3D and 2D modes [42, 38, 39, 34].

Finally, in order to understand how the stationary regimes are sustained, we study the helical decomposition of the energy flux. In Fig. 6 we present the homochiral and heterochiral contributions on the total energy flux of PRJ-A1, PRJ-A3 and PRJ-A6 (which have $\Omega = 0$, $\Omega = 40$ and $\Omega = 160$, respectively). It is interesting to observe that for the case of strong rotation the stationary state is the result of the non-trivial cancellation of the homo and heterochiral channels. So while the total flux is zero, this is achieved by the dynamical balance of the channels that bring energy forwards (the heterochiral) and the ones that bring it backwards (the homochiral). The same phenomenon has been observed in flows composed by a combination of 2D3C (two dimension, three component) flows [44]. The amplitude and range of modes that are involved in this flux balance does depend slightly on the rotation rate, with simulation PRJ-A3 being the one with the largest number of modes that had non-zero flux in the homo and heterochiral channels.

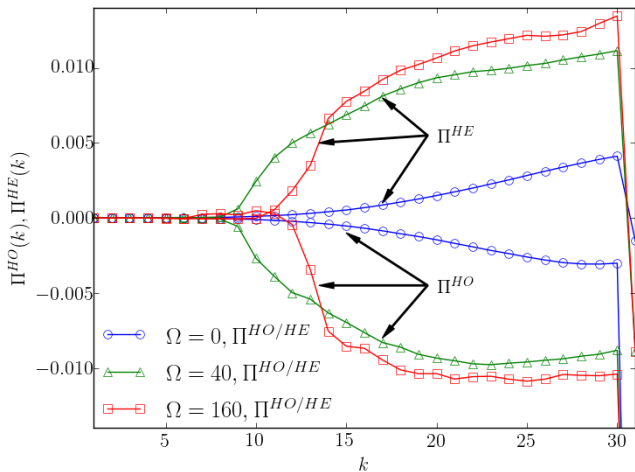


Fig. 6. Homo and heterochiral contributions to the total energy flux, $\Pi^{HO}(k)$ and $\Pi^{HE}(k)$ respectively, of simulations PRJ-A1, PRJ-A3, and PRJ-A6.

4 Conclusions

By performing simulations of rotating turbulence in which modes perpendicular to the rotation axis (the 2D modes) were conservatively removed we were able to assess the

role of the 3D modes in the formation of the inverse cascade. We showed that while a stationary inverse cascade is not formed, energy is nonetheless transferred to the low wavenumber modes. The resulting non-trivial energy distribution is (i) strongly anisotropic, concentrated close to the (removed) 2D plane and (ii) highly peaked around $|k| \sim 10$. Moreover, and more importantly, we show that the stationary state is reached due to a balance between homochiral and heterochiral transfers. The former transferring energy backward and the latter forward.

In short, while the 2D modes are essential in order to have an inverse cascade, the 3D modes play a non-negligible role distributing the energy towards the large scales and in an anisotropic fashion.

The Fourier space decomposition in 2D-manifold and waves-component has been performed also in small Rossby number turbulence confined in two infinite walls perpendicular to the rotation axis, in this configuration results show that the two-dimensional component has no effect on the wave-component energetics [52]. Another study on rotating turbulence in a triple-periodic domain, instead, claimed that the backward energy cascade cannot be simplified as a 2D dynamics, but it supports the picture that 3D-waves near resonant interactions efficiently transfer energy from 3D modes to larger-scale 2D modes [43].

It is important to comment about a recent study where a similar problem is addressed [18] by damping the 2D slow modes instead of decimating them as we do here. By doing this, the presence of three dimensional inertial waves is enhanced and energy is accumulated at small scales, indicating a more efficient forward energy cascade once the 2D modes become unavailable because of the strong damping. Different from our case, in [18] the system is forced at large scale thus not allowing for the energy to flow backwards. Both works suggest that there is a non-trivial correlation between 2D and 3D dynamics.

Acknowledgments

The research leading to these results has received funding from the European Union's Seventh Framework Programme (FP7/2007-2013) under grant agreement No. 339032. The authors acknowledge Alexandros Alexakis for very useful discussions and comments.

Authors contribution statement

All the authors were involved in the preparation of the manuscript. All the authors have read and approved the final manuscript.

References

1. U. Frisch. *Turbulence: the legacy of A.N. Kolmogorov*. Cambridge University Press, Cambridge, [Eng.] ; New York, 1995.

2. Pierre Sagaut and Claude Cambon. *Homogeneous Turbulence Dynamics*. Springer, 2018.
3. Stephen B Pope. *Turbulent flows*. Cambridge University Press, 2000.
4. P. A. Davidson. *Turbulence in Rotating, Stratified and Electrically Conducting Fluids*. Cambridge University Press, September 2013.
5. Robert H. Kraichnan. Inertial ranges in two-dimensional turbulence. *Physics of Fluids*, 10:1417–1423, 1967.
6. Leslie M. Smith, Jeffrey R. Chasnov, and Fabian Waleffe. Crossover from two- to three-dimensional turbulence. *Phys. Rev. Lett.*, 77(12):2467–2470, 1996.
7. P. D. Mininni and A. Pouquet. Helicity cascades in rotating turbulence. *Phys. Rev. E*, 79(2):026304, 2009.
8. P. D. Mininni, A. Alexakis, and A. Pouquet. Scale interactions and scaling laws in rotating flows at moderate rossby numbers and large reynolds numbers. *Phys. Fluids*, 21(1):015108, 2009.
9. G. D. Nastrom, K. S. Gage, and W. H. Jasperson. Kinetic energy spectrum of large-and mesoscale atmospheric processes. *Nature*, 310(5972):36–38, 1984.
10. Antonio Celani, Stefano Musacchio, and Dario Vincenzi. Turbulence in more than two and less than three dimensions. *Physical Review Letters*, 104(18):184506, 2010.
11. Hussein Aluie, Matthew Hecht, and Geoffrey K. Vallis. Mapping the energy cascade in the north atlantic ocean: The coarse-graining approach. *Journal of Physical Oceanography*, 48(2):225–244, 2017.
12. Alexandros Alexakis, Pablo D. Mininni, and Annick Pouquet. On the inverse cascade of magnetic helicity. *The Astrophysical Journal*, 640(1):335, 2006.
13. P. D. Mininni. Inverse cascades and α effect at a low magnetic prandtl number. *Physical Review E*, 76(2):026316, 2007.
14. Luca Biferale, Stefano Musacchio, and Federico Toschi. Inverse energy cascade in three-dimensional isotropic turbulence. *Physical Review Letters*, 108(16):164501, 2012.
15. L. Biferale, S. Musacchio, and F. Toschi. Split energy-helicity cascades in three-dimensional homogeneous and isotropic turbulence. *Journal of Fluid Mechanics*, 730:309–327, 2013.
16. Alexandros Alexakis. Helically decomposed turbulence. *Journal of Fluid Mechanics*, 812:752–770, 2017.
17. James YK Cho, Kristen Menou, Bradley MS Hansen, and Sara Seager. Atmospheric circulation of close-in extrasolar giant planets. i. global, barotropic, adiabatic simulations. *The Astrophysical Journal*, 675(1):817, 2008.
18. Thomas Le Reun, Benjamin Favier, Adrian J. Barker, and Michael Le Bars. Inertial wave turbulence driven by elliptical instability. *Phys. Rev. Lett.* 119(3):034502, 2017.
19. Horia Dumitrescu and Vladimir Cardos. Rotational effects on the boundary-layer flow in wind turbines. *AIAA journal*, 42(2):408–411, 2004.
20. A. Sen, P. D. Mininni, D. Rosenberg, and A. Pouquet. Anisotropy and nonuniversality in scaling laws of the large-scale energy spectrum in rotating turbulence. *Phys. Rev. E*, 86:036319, Sep 2012.
21. L. Biferale, F. Bonaccorso, I.M. Mazzitelli, M.A.T. van Hinsberg, A.S. Lanotte, S. Musacchio, P. Perlekar, and F. Toschi. Coherent structures and extreme events in rotating multiphase turbulent flows. *Physical Review X*, 6(4):041036, 2016.
22. E. Horne and P. D. Mininni. Sign cancellation and scaling in the vertical component of velocity and vorticity in rotating turbulence. *Physical Review E*, 88(1):013011, 2013.
23. F. Moisy, C. Morize, M. Rabaud, and J. Sommeria. Decay laws, anisotropy and cycloneanticyclone asymmetry in decaying rotating turbulence. *J. Fluid Mech.*, 666:5–35, January 2011.
24. C. Cambon and L. Jacquin. Spectral approach to non-isotropic turbulence subjected to rotation. *J. Fluid Mech.*, 202:295–317, 1989.
25. C. Cambon, N. N. Mansour, and F. S. Godeferd. Energy transfer in rotating turbulence. *J. Fluid Mech.*, 337:303–332, 1997.
26. S. Nazarenko. *Wave Turbulence*. Springer, 1 edition, February 2011.
27. A. C. Newell. Rossby wave packet interactions. *J. Fluid Mech.*, 35(02):255–271, January 1969.
28. S. Galtier. Weak inertial-wave turbulence theory. *Phys. Rev. E*, 68(1):015301, July 2003.
29. Qiaoning Chen, Shiyi Chen, Gregory L. Eyink, and Darryl D. Holm. Resonant interactions in rotating homogeneous three-dimensional turbulence. *Journal of Fluid Mechanics*, 542:139–164, 2005.
30. E. Yarom and E. Sharon. Experimental observation of steady inertial wave turbulence in deep rotating flows. *Nature Physics*, 10(7):510–514, June 2014.
31. A. Campagne, B. Gallet, F. Moisy, and P.-P. Cortet. Disentangling inertial waves from eddy turbulence in a forced rotating turbulence experiment. *Phys. Rev. E* 91, 043016 (2015).
32. P. Clark di Leoni, P. J. Cobelli, P. D. Mininni, P. Dmitruk, and W. H. Matthaeus. Quantification of the strength of inertial waves in a rotating turbulent flow. *Phys. Fluids*, 26(3):035106, March 2014.
33. P. Clark di Leoni, P. D. Mininni, and M. E. Brachet. Spatiotemporal detection of Kelvin waves in quantum turbulence simulations. *Phys. Rev. A*, 92(6):063632, December 2015.
34. P. Clark di Leoni and P. D. Mininni. Quantifying resonant and near-resonant interactions in rotating turbulence. *J. Fluid Mech.*, 809:821–842, December 2016.
35. F. Waleffe. Inertial transfers in the helical decomposition. *Phys. Fluids A*, 5(3):677, 1993.
36. Michele Buzzicotti, Hussein Aluie, Luca Biferale, and Moritz Linkmann. Energy transfer in turbulence under rotation. *arXiv preprint arXiv:1711.07054*, 2017.
37. L. Jacquin, O. Leuchter, C. Cambon, and J. Mathieu. Homogeneous turbulence in the presence of rotation. *J. Fluid Mech.*, 220:1–52, November 1990.
38. A. Alexakis. Rotating taylor–green flow. *J. Fluid Mech.*, 769:46–78, 2015.
39. B. Gallet. Exact two-dimensionalization of rapidly rotating large-Reynolds-number flows. *J. Fluid Mech.*, 783:412–447, November 2015.
40. E. Calzavarini, C. R. Doering, J. D. Gibbon, D. Lohse, A. Tanabe, and F. Toschi. Exponentially growing solutions in homogeneous rayleigh-bénard convection. *Phys. Rev. E* 73, 035301 (2006).
41. F. Bellet, F. S. Godeferd, J. F. Scott, and C. Cambon. Wave turbulence in rapidly rotating flows. *J. Fluid Mech.* 562, 83 (2006).
42. L. M. Smith and F. Waleffe. Generation of slow large scales in forced rotating stratified turbulence. *J. Fluid Mech.*, 451:145–168, January 2002.

43. Leslie M Smith and Youngsuk Lee. On near resonances and symmetry breaking in forced rotating flows at moderate rossby number. *Journal of Fluid Mechanics*, 535:111–142, 2005.
44. L. Biferale, M. Buzzicotti, and M. Linkmann. From two-dimensional to three-dimensional turbulence through two-dimensional three-component flows. *Physics of Fluids*, 29(11):111101, 2017.
45. HP Greenspan. Theory of rotating fluids, CUP Archive, Cambridge (1968).
46. HP Greenspan. On the non-linear interaction of inertial modes. *Journal of Fluid Mechanics*, 36(2):257–264, 1969.
47. Pedro F Embid and Andrew J Majda. Low froude number limiting dynamics for stably stratified flow with small or finite Rossby numbers. *Geophysical & Astrophysical Fluid Dynamics*, 87(1-2):1–50, 1998.
48. Leslie M Smith and Fabian Waleffe. Transfer of energy to two-dimensional large scales in forced, rotating three-dimensional turbulence. *Physics of fluids*, 11(6):1608–1622, 1999.
49. Ganapati Sahoo and Luca Biferale. Energy cascade and intermittency in helically decomposed navier–stokes equations. *Fluid Dynamics Research*, 50(1):011420, 2018.
50. F. Waleffe. The nature of triad interactions in homogeneous turbulence. *Physics of Fluids A: Fluid Dynamics (1989-1993)*, 4(2):350–363, February 1992.
51. Peter Constantin and Andrew Majda. The beltrami spectrum for incompressible fluid flows. *Communications in mathematical physics*, 115(3):435–456, 1988.
52. Julian F Scott. Wave turbulence in a rotating channel. *Journal of Fluid Mechanics*, 741:316–349, 2014.